A FINITE ELEMENT ANALYSIS OF INTACT AND IMPLANTED FEMUR BEHAVIOUR DIRING ROUTINE ACTIVITIES

22 – 2001

Preprint, no 22 – 01 / 2001

Department of Computer Science
University of Ioannina
45110 Ioannina, Greece

A FINITE ELEMENT ANALYSIS OF INTACT AND IMPLANTED FEMUR BEHAVIOUR DURING ROUTINE ACTIVITIES

V.A. Papathanasopoulou[1], D.I. Fotiadis[2] and C.V. Massalas[3]
[1]Medical Physics Laboratory, Medical School, University of Ioannina, GR 451 10 Ioannina, Greece
[2]Dept. of Computer Science, University of Ioannina, GR 451 10 Ioannina, Greece
[3]Dept. of Materials Science and Engineering, University of Ioannina, GR 451 10 Ioannina, Greece

Keywords: Human femur modelling; Strain distribution; Intact femur; Implanted femur; Stress-shielding.

Word Count: 2563 (references, tables, figures, table and figure captions excluded)

Corresponding Author: Prof. Dimitrios I. Fotiadis,
Dept. of Computer Science,
Medical Technology and Intelligent Information Systems Unit,
University of Ioannina,
GR 451 10 Ioannina,
Greece.
Phone: +30-651-98803, Fax: +30-651-97092
Email: fotiadis@cs.uoi.gr

Abstract

A mapping of the strain situation in an intact and an implanted femur model with a subsequent verification of the stress shielding effect is presented for nine different routine activities (slow walking, normal walking, fast walking, up stairs walking, down stairs walking, standing up, sitting down, standing on 2-1-2 legs, and knee bend). A three-dimensional finite element model of the human femur is developed and a femoral endoprosthesis is inserted in the femur model. A point hip joint reaction force at the moment of peak hip joint reaction is employed, while the distal end of the femur is constrained in translation only. Principal strains in the surface of the models and at nodal positions of the bone-implant interface are computed. It appears that the heaviest loading occurs in the up stairs loading case, where stress shielding is more prominent as well. Stress shielding is stronger in the area of transition from the upper epiphysis to the diaphysis and decreases along the diaphysis.

1. Introduction

The load-transfer mechanism from prosthesis to bone is one of the most important issues in a total hip arthroplasty (THA). Excessive stresses are responsible for fatigue failure of components or disruption of the implant/bone fixation [1]. Lower than normal stresses due to "stress-shielding" and adaptive bone remodeling may cause bone resorption around femoral hip stems with subsequent loosening, threatening the long-term integrity of the implant [2,3,4]. The introduction of wear debris into the bone-implant interface and the relative motion across the interface are other causes of loosening [5]. The cementless fixation of the implant employing direct bone-prosthesis contact offers an alternate technique in the attempt to overcome the problems associated with the cement. In all cases, the quality of the initial fit is critical since fixation requires intimate contact along the interface [6]. The study of stress patterns

generated by the load-transfer mechanism and the understanding of their relationships with loading characteristics, prosthetic design, materials, and fixation characteristics, is critical in facing the issue of implant stability.

Several investigators have studied the strain and stress distribution in intact and implanted femurs and verified the existence of stress-shielding during instances of the gait cycle or arbitrary loading conditions [6,7,8]. A solution to the shielding problem would be a prosthesis which loads the femur in a manner as similar as possible to the natural state. Before validating a certain prosthesis design, a careful analysis of the stresses in an intact and an implanted bone should be made under a variety of as many realistic-simulating boundary conditions as possible.

In this paper, the effect of various types of realistic loading during routine activities to the load transferred to the femur across a fixed bone-prosthesis interface, at the moment of peak loading, is studied. The routine activities include slow walking, normal walking, fast walking, up stairs walking, down stairs walking, standing up, sitting down, standing on 2-1-2 legs, and knee bend. In the literature, there exist articles on the stress and/or strain distribution pattern of the femur and the femur-prosthesis interface during gait and/or arbitrary loading conditions [6,7,8,9,10,11], but, to our knowledge, no comparative study among the nine forementioned activities has been presented up to now. A quasi-static model of the human femur is employed using the three-dimensional finite element approach and boundary conditions derived from the literature [12]. A three-dimensional solid finite element model of an intact human femur is constructed assuming linear elastic, isotropic and homogeneous material properties. The geometry of the model is obtained from the three-dimensional reconstruction of the periosteal contours of transverse CT images of a human cadaver femur. The femoral head is then removed from the above model and a designed prosthesis has been nailed inside the model, simulating a cementless case. The force at the

moment of peak loading exerted by the hip joint on the femoral head or the superior end of the prosthesis, is applied at a point location of both models. The distal end of the femur is constrained only in translation. A distinction of the bone material properties in the diaphysis and epiphyses is accounted for. Nine different loading conditions are considered based on published recorded kinematic data of the hip joint reaction force during various routine activities [12]. The principal surface strain distribution in the intact and the implanted femur models during the instant of peak hip joint reaction force is obtained and compared in all nine cases. The maximum and minimum principal strain values at nodal positions along the femoral axis at the bone-implant interface surfaces are computed and compared in all cases. The results are indicative of the stress-shielding effect occuring in implanted femurs during a variety of routine activities. It is evident that three-dimensional finite element models employing realistic loading conditions could prove useful in the mapping of the mechanical environment in bones, with subsequent practical applications in the improvement of prosthesis design and implementation of therapeutic methods.

2. Materials and Methods

2.1. Femur model geometry

The geometry of the femur was obtained by 3-D reconstruction of the periosteal contours of 2 mm thickness transverse CT slices of a human femoral bone. The length of the femur was approximately 350 mm and the diameter of the femoral head was around 40 mm.

2.2. Finite element model

A 3-D finite element model was generated using the Patran 8.5 Software (MSC Software Corporation). A solid mesh of the intact femur was constructed consisting of 5584 tetrahedral elements and 1393 nodes.

The global element edge length was 7.5 mm. In the model of the nailed femur 4593 tetrahedral elements were employed for the bone-prosthesis system. The contact between bone and the prosthesis was modelled using surface elements. The inner surface of the femoral shaft was meshed with 530 triangular elements, resulting in a total of 5124 elements and 1099 nodes for the bone-implant system, after equivalencing. Friction between bone and the prosthesis was neglected.

2.3. Material properties

The femur was modelled as a linear elastic, isotropic and homogeneous material. The material properties were distinguished between two principal regions, namely, trabecular bone at the epiphyses and cortical bone in the diaphysis [13] (Table 1). The values of the assigned cortical bone properties are lower than their average values in human cortical femoral bone. This was done in order to compensate for the lack of existence of the trabecular bone portion present in the diaphysis and of the medullary canal.

The titanium alloy used for the prosthesis material was assumed to be linear elastic, isotropic and homogeneous (Table 1).

2.4. Boundary conditions

Nine different common activities that cause high hip joint loads were investigated (Table 2) in both an intact and an implanted femur model. The hip-joint contact force data correspond to the instant of peak hip contact force during the gait cycle, which reflects in mechanical terms a worst case scenario for the behaviour of the bone-implant system. The data were derived from Bergmann *et al.* [12] and are "typical" results calculated with a mathematical averaging procedure from the data of various trials and patients with instrumented hip implants.

The magnitude and orientation of the force components were defined with respect to a right-handed cartesian coordinate system for the right femur with its origin at the center of the femoral head in the

intact femur model and a corresponding position in the implanted femur model (Fig. 1). The +x-axis pointed medially, the +y-axis posteriorly and the +z-axis was directed superiorly. The resultant hip joint reaction force was applied on the near-hemispherical surface of the acetabulum-femoral head contact area of the intact femur. In the implanted femur the resultant force was applied on the top of the prosthesis neck. The body weight was taken as 75 kg.

The distal end of the femur, at the location of the knee joint was constrained in translation.

2.5. Computations

Hip-joint contact forces were applied quasi-statically to represent the gait cycle. Nine runs were done for each of the intact and the implanted femur models, respectively, at the instant of peak hip contact force.

Principal strains were selected to represent the femur load state sufficiently. The principal surface strain distributions in the intact and the implanted femur were compared under the nine loading activities. The loading of the implant was assessed by the principal strain values along lines in the bone-implant interface.

The analysis was performed using the Nastran package (Nastran 70.5 MSC Software Corporation) on a Silicon Graphics Origin 2000 Computer (16 CPUs, 3.2 GB Memory).

3. Results

A mapping of the principal surface strain distribution in the intact femur model at the moment of peak hip contact force during the nine activities of Table 2 is shown in Fig. 2. The corresponding distribution in the implanted femur model is shown in Fig. 3. The maximum principal surface strain ranges in both models are tabulated in Table 3. The greatest maximum principal surface strains in both models occur during the

up-stairs walking, followed by the down-stairs walking. The lowest maximum principal surface strains occur during knee bend in the intact femur model and during standing on 2-1-2 legs in the implanted one. The maximum and minimum principal strain values at the medial, lateral, anterior and posterior surfaces of the bone-implant interface during the nine activities are plotted in Fig. 4. The points of strain registration correspond to the nodal positions along a line in the superior-inferior direction of the femur at the corresponding surfaces.

A comparison between the maximum principal strain values at the nodal positions of the anterior surface of the bone-implant interface and at corresponding points of the intact femur model at the moment of peak hip contact force in walking is illustrated in Fig. 5.

4. Discussion

The strain and stress distribution and the existence of stress-shielding in implanted femurs have been addressed by several researchers [6,7,8]. The boundary conditions employed commonly involve the hip joint and muscle forces applied vectorially as point forces during a single or various instances of the gait cycle. The present study focuses on the comparison of the principal strains between an intact and an implanted finite element femur model at the instant of maximum hip contact pressure during nine different routine activities. The computations verify the presence and compare the intensity of stress shielding in the different loading patterns. A detailed discussion on the principal surface strains in both models and the strains at the bone-implant interface is analytically given below.

Surface strains

The greatest range of maximum principal surface strains occurs in the up-stairs walking load case in both models.

The surface strains in the intact and the implanted femur models differ by about one order of magnitude, the strains in the implanted femur being lower. This is indicative of the stress-shielding effect in implanted bones.

As shown in Fig. 3, in the implanted femur model the greatest principal surface strains occur on the anterior surface of the femur during (a), (b), (c), (d) and (e). In (f), (g) and (i) they move towards the medial surface of the mid-lower diaphysis, whereas in (h) the greatest strains appear on the lateral surface of the mid-upper diaphysis. Quite different is the situation in the intact femur model. As shown in Fig. 2, the greatest principal surface strains occur on the anterior surface of the lower epiphysis during (a) to (f). In (g) and (i) the maximum strains move to the medial part of the lower epiphysis. In (h), the region between the femoral head and the greater trochanter experiences the higher strains in addition to the anterior part of the lower epiphysis.

Strains at the bone-implant interface

As shown in Fig. 4, the higher maximum strains occur in the anterior surface of the bone-implant interface, followed by those at the lateral, posterior and medial surfaces.

Medial strains

The higher maximum and minimum principal strains occur when standing on 2-1-2 legs and the lower ones in the sitting down and knee bend load cases. In other words, the greatest range of principal strain values appears when standing on 2-1-2 legs and the lowest one when sitting down and knee bending.

There is no great variation of medial strains in the superior-inferior direction. The lower minimum strains appear between 105 and 140 mm in the superior-inferior direction, in all load cases except for (g) and (i) where they appear between 75 and 110 mm.

Lateral strains

The higher maximum and minimum principal strains occur in the up-stairs walking. The greatest range of principal strains appears in the up-stairs walking, followed by down-stairs walking and fast walking. In general, there is an increase of the maximum and decrease of the minimum principal strains, when moving from the upper epiphysis towards the diaphysis. This pattern is not followed in the case of standing up where the maximum strain remains almost constant, and the cases of sitting down and knee bend where the maximum strain drops at around 42 mm.

Anterior strains

The higher maximum and minimum principal strains occur in the up-stairs walking. In general, there is an initial decrease and subsequent increase (at 55 mm) of the maximum principal strains, when moving from the upper epiphysis towards the diaphysis. The minimum principal strains are nearly constant initially and at around 70 mm they start increasing.

Superior strains

The higher maximum and minimum principal strains occur in the up-stairs walking. In the epiphysis the maximum and minimum principal strains are nearly constant and they start increasing at around 70 mm.

Anterior strains at intact and implanted femur

The maximum principal strain values at the nodal positions of the anterior surface of the bone-implant interface along the long axis of the femur are lower in comparison to those in the intact femur model at the location of epiphysis and upper diaphysis (up to around 95 mm) as shown in Fig. 5. This is in accordance with the expected pattern due to the stress-shielding effect.

The above findings are qualitatively and quantitatively comparable to those of Duda *et al.* [9], McNamara *et al.* [6], Cristofolini *et al.* [10], and Walker *et al.* [8]. Stress-shielding is shown to occur along the entire

surface of the intact and implanted models, and is more prominent in the up-stairs loading case, which is also the worst case in terms of loading. The antero-lateral surfaces of the bone-implant interface are more heavily loaded in comparison to the postero-medial surfaces, at the moment of peak hip joint contact force. Stress-shielding is stronger at the transition zone from the upper epiphysis to the diaphysis and becomes less important along the inferior diaphysis.

The present work shows that three-dimensional finite element analysis is a useful tool in the mapping of the stress-strain environment in the human femur during various activities. The model can be generalised to various types of loading and instances of the gait cycle. Further work should be undertaken on a model with more realistic constraints such as the inclusion of the several different muscle groups applied during different instances of the gait cycle. A verification of such a model with experimental data, could lead to the improvement in the design of intramedullary prostheses in relation to the reduction of the stress shielding effect.

Acknowledgements

We thank Iraklis Kourtis and Lambros Kourtis for their help in the construction of the femur and prosthesis geometry. This work is partially supported by the IST-2000-26350 project "USBONE: A remotely monitored wearable ultrasound device for the monitoring and acceleration of bone healing".

References

[1] Huiskes, R., Weinans, H., and Dalstra, M. (1989) Adaptive bone remodeling and biomechanical design considerations for noncemented total hip arthroplasty. *Orthopedics* **12**, 1255-1267.

[2] Huiskes, R., Weinans, H., and Van Rietbergen, B. (1992) The relationship between stress shielding and bone resorption around total hip stems and the effects of flexible materials. *Clinical Orthopedics* **272**, 124-134.

[3] Toni, A., McNamara, B., Viceconti, M., Sudanese, A., Baruffaldi, F., and Giunti, A. (1996) Bone remodelling after total hip arthroplasty. *Journal of Materials Science: Materials in Medicine* **7**, 149-152.

[4] Van Rietbergen, B., Huiskes, R., Weinans, H., and Sumner, D. R. (1992) ESB Research Award 1992. The mechanism of bone remodeling and resorption around press-fitted THA stems. *Journal of Biomechanics* **26**, 369-382.

[5] Joshi, M. G., Advani, S. G., Miller, F., and Santare, M. H. (2000) Analysis of a femoral hip prosthesis designed to reduce stress shielding. *Journal of Biomechanics* **33**, 1655-1662.

[6] McNamara, B. P., Cristofolini, L., Toni, A., and Taylor, D. (1997) Relationship between bone-prosthesis bonding and load transfer in total hip reconstruction. *Journal of Biomechanics* **30**, 621-630.

[7] Cristofolini, L., Cappello, A., McNamara, B. P., and Viceconti, M. (1996) A minimal parametric model of the femur to describe axial elastic strain in response to loads. *Medical Engineering and Physics* **18**, 502-514.

[8] Walker, P. S., Schneeweist, D., Murphy, S., and Nelson, P. (1987) Strains and micromotions of press-fit femoral stem prostheses. *Journal of Biomechanics* **20**, 693-702.

[9] Duda, G. N., Heller, M., Albinger, J., Schulz, O., Schneider, E., and Claes, L. (1988) Influence of muscle forces on femoral strain distribution. *Journal of Biomechanics* **31**, 841-846.

[10] Cristofolini, L., Viceconti, M., Toni, A., and Giunti, A. (1995) Influence of thigh muscles on the axial strains in a proximal femur during early stance in gait. *Journal of Biomechanics* **28**, 617-624.

[11] Taylor, M. E., Tanner, K. E., Freeman, M. A. R., and Yettram, A. L. (1996) Stress and strain distribution within the intact femur: compression or bending?,*Medical Engineering and Physics* **18**, 122-131.

[12] Bergmann, G., Deuretzbacher, G., Heller, M., Graichen, F., Rohlmann, A., Strauss, J., and Duda, G. N. (2001) Hip contact forces and gait patterns from routine activities. *Journal of Biomechanics* **34**, 859-871.

[13] Yuehuei, A. H. (2000) Mechanical testing of bone and the bone-implant interface. In: Yuehuei, A. H., Draughn, R. A. (Eds.), *Mechanical properties of bone*. CRC Press, pp.41-63.

Table 1

Material properties for bone and prosthesis

Property	Cortical Bone[13]	Trabecular Bone[13]	Titanium Alloy [13]
Young's modulus	15 GPa	0.7 GPa	110 GPa
Poisson's ratio	0.33	0.2	0.3
Density	1650 kg/m^3	620 kg/m^3	4700 kg/m^3

Table 2

Hip contact force coordinates in nine different activities, at the instant of peak hip contact force, in the femur coordinate system[a]

Activity	Peak hip contact force components
Slow walking	[49, 32, 228]
Normal walking	[55, 30, 225]
Fast walking	[53, 32, 244]
Up stairs	[57, 57, 238]
Down stairs	[58, 40, 250]
Standing up	[55, 20, 182]
Sitting down	[50, 0, 150]
Standing on 2-1-2 legs	[30, 12, 224]
Knee bend	[45, 5, 140]

[a] The numbers in the brackets are multipliers of % the body weight (%BW)

Table 3

Maximum principal surface strain ranges in the intact and the implanted femur models

Activity	*Intact femur model*	*Implanted femur model*
Slow walking	4.48×10^{-3} - 6.72×10^{-2}	4.13×10^{-4} - 6.19×10^{-3}
Normal walking	4.26×10^{-3} - 6.39×10^{-2}	3.95×10^{-4} - 5.92×10^{-3}
Fast walking	4.49×10^{-3} - 6.73×10^{-2}	4.19×10^{-4} - 6.28×10^{-3}
Up stairs	8.02×10^{-3} - 1.20×10^{-1}	6.79×10^{-4} - 1.02×10^{-2}
Down stairs	5.64×10^{-3} - 8.45×10^{-2}	5.05×10^{-4} - 7.58×10^{-3}
Standing up	3.68×10^{-3} - 5.51×10^{-2}	3.37×10^{-4} - 5.06×10^{-3}
Sitting down	2.99×10^{-3} - 4.18×10^{-2}	2.66×10^{-4} - 3.98×10^{-3}
Standing on 2-1-2 legs	1.92×10^{-3} - 2.88×10^{-2}	4.05×10^{-4} - 6.07×10^{-3}
Knee bend	2.70×10^{-3} - 4.04×10^{-2}	2.34×10^{-4} - 3.51×10^{-3}

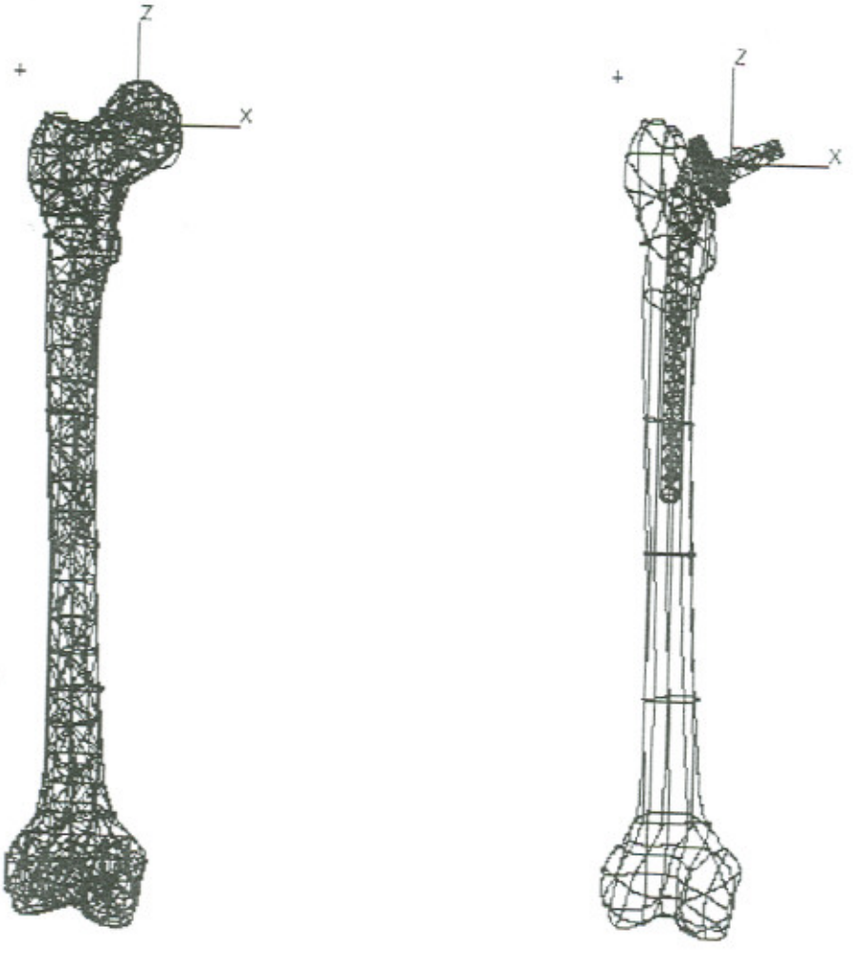

Fig.1. Femur coordinate system in intact and implanted femur models

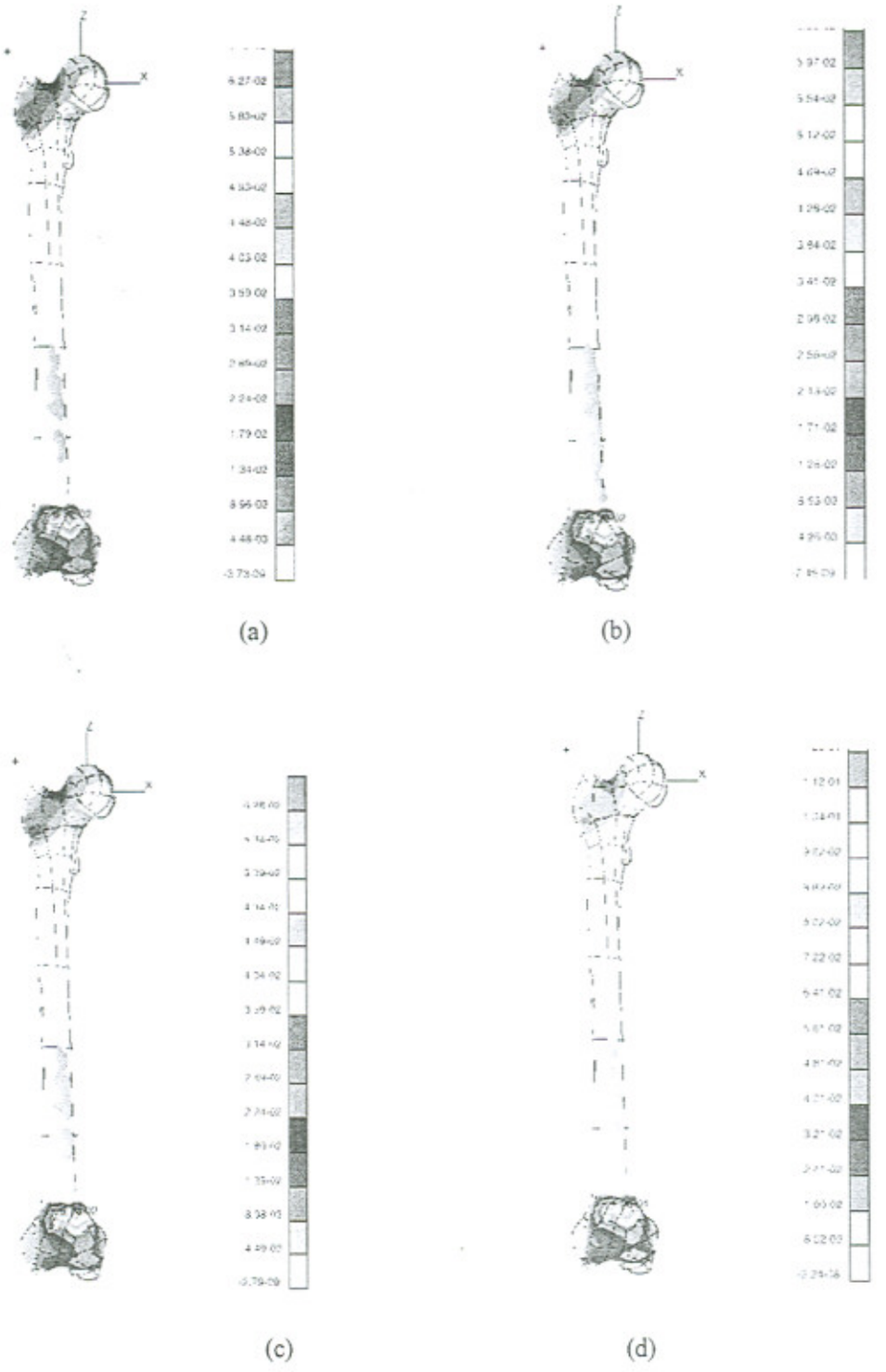

Fig. 2. Maximum principal surface strain distribution in the intact femur model at the moment of peak hip contact force during (a) slow walking, (b) normal walking, (c) fast walking, (d) up stairs walking

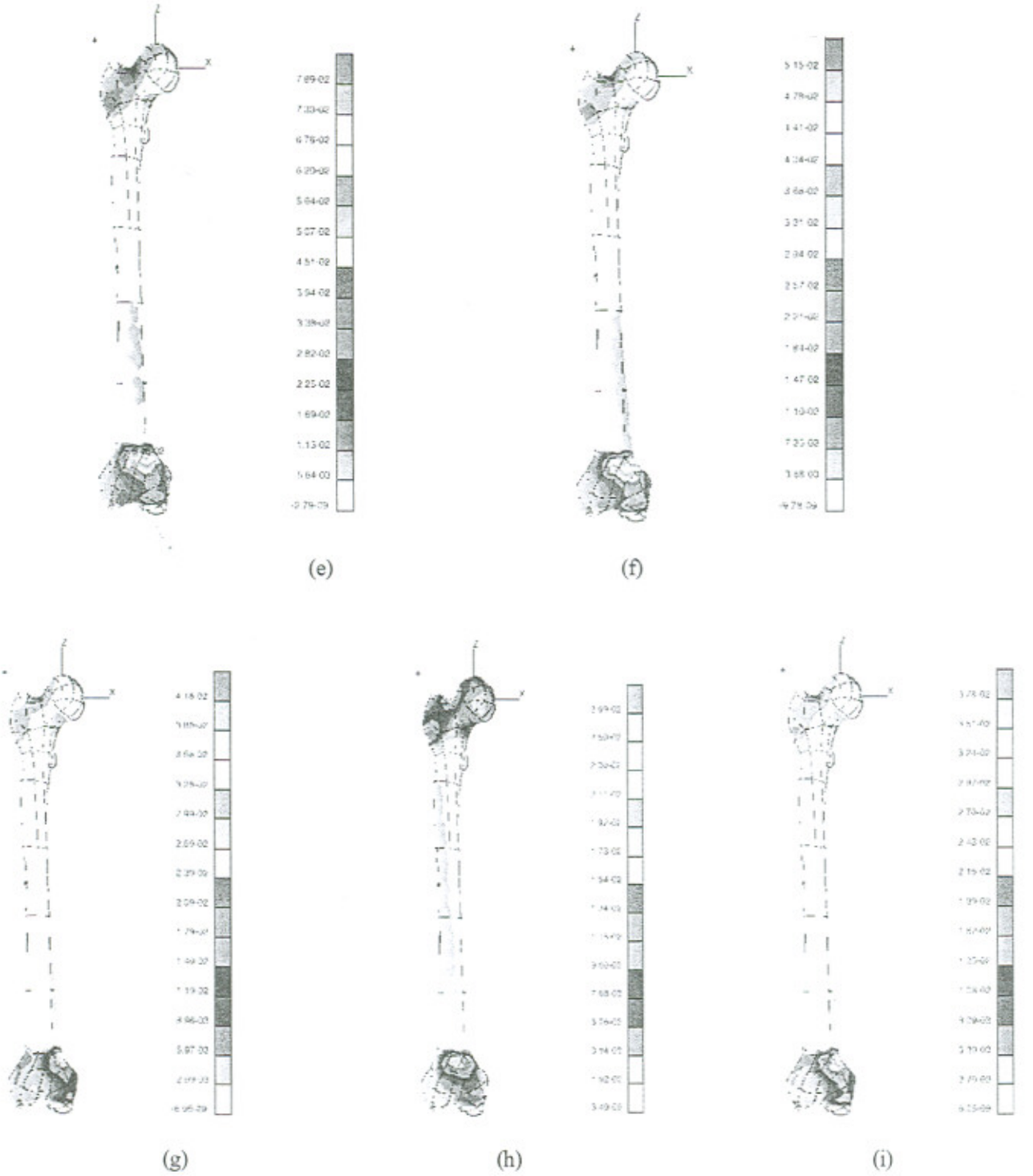

Fig. 2. (continued) Maximum principal surface strain distribution in the intact femur model at the moment of peak hip contact force during (e) down stairs walking, (f) standing up, (g) sitting down, (h) standing on 2-1-2 legs, and (i) knee bend.

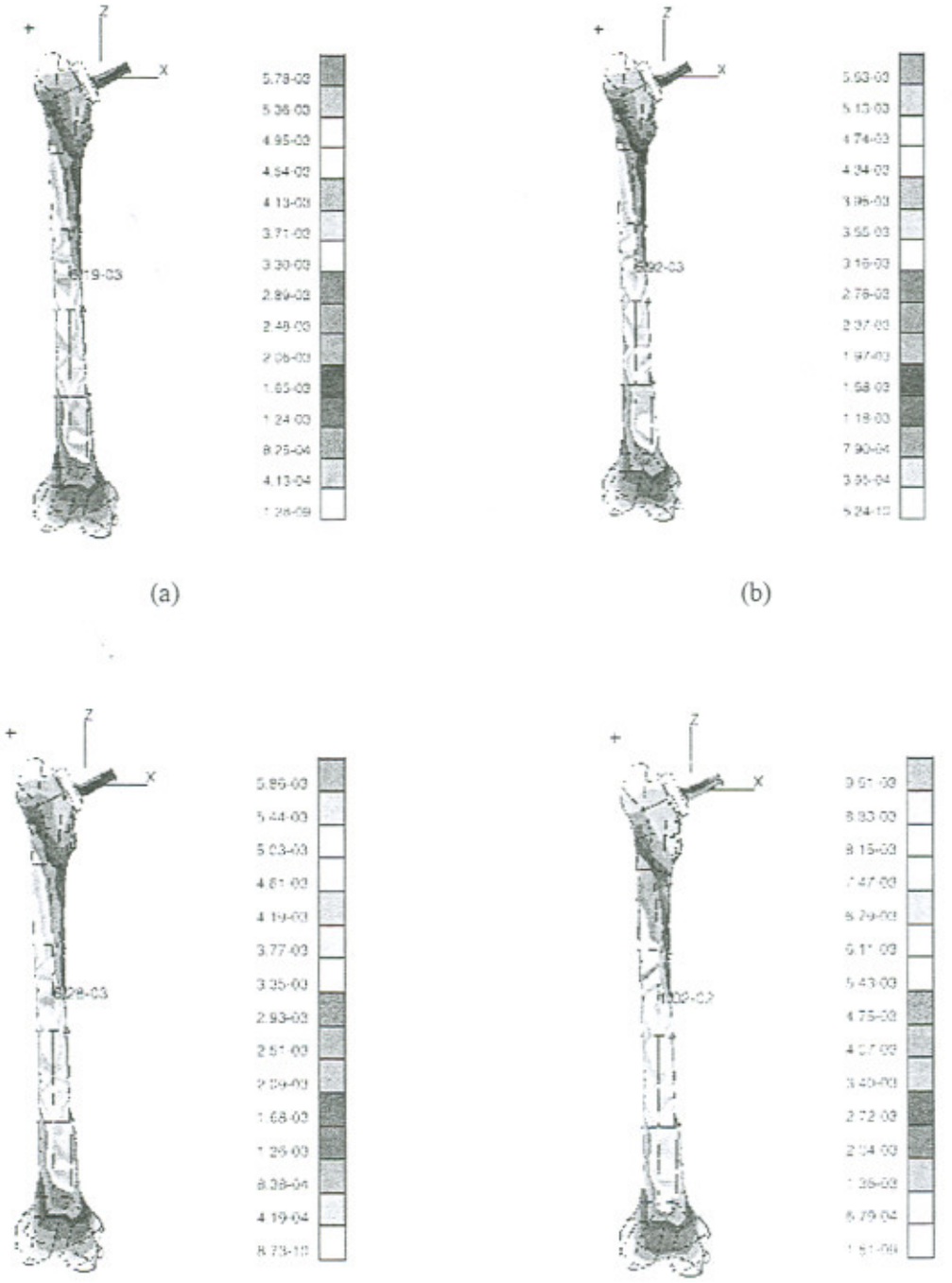

Fig. 3. Maximum principal surface strain distribution in the implanted femur model at the moment of peak hip contact force during (a) slow walking, (b) normal walking, (c) fast walking, (d) up stairs walking.

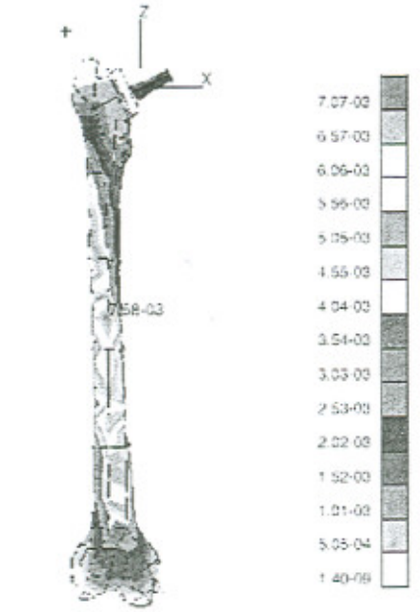

(e)

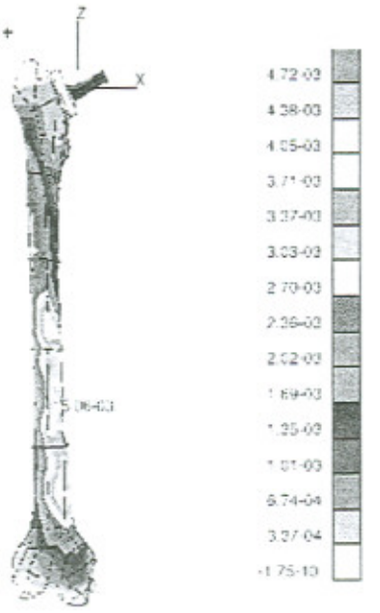

(f)

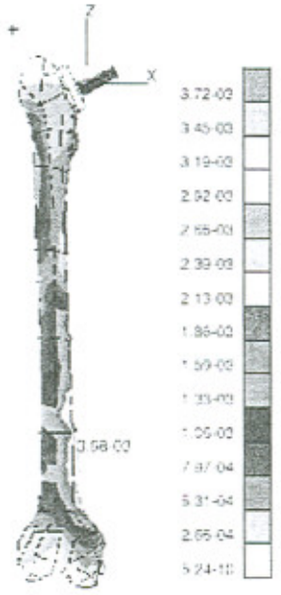

(g)

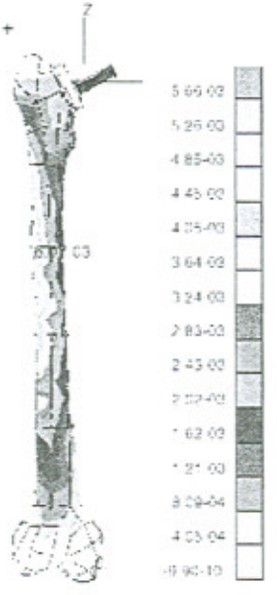

(h)

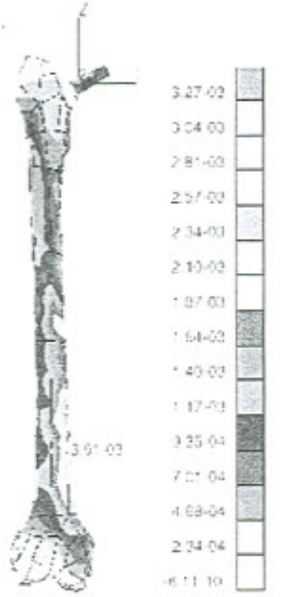

(i)

Fig. 3. (continued) Maximum principal surface strain distribution in the implanted femur model at the moment of peak hip contact force during (e) down stairs walking, (f) standing up, (g) sitting down, (h) standing on 2-1-2 legs, and (i) knee bend.

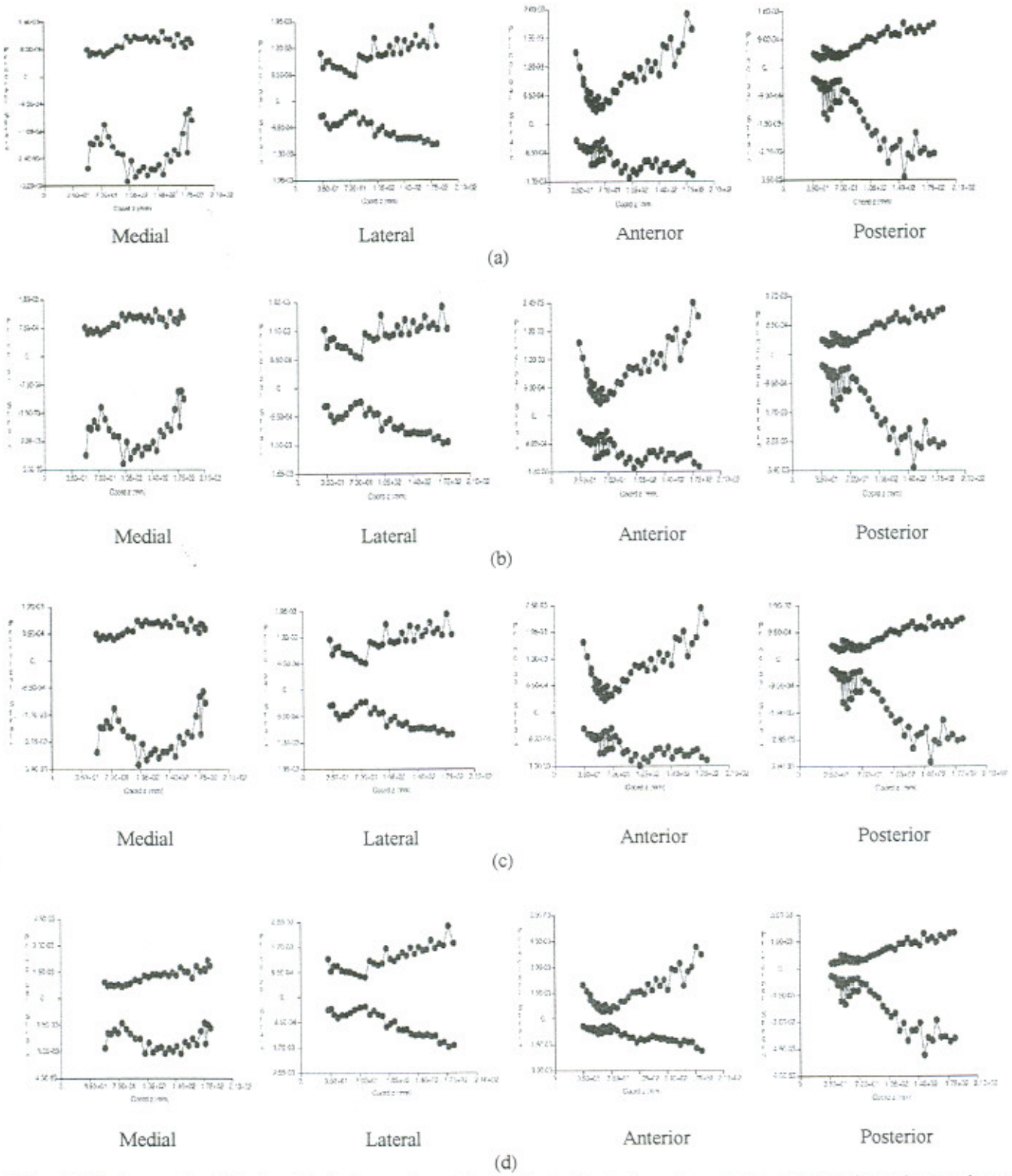

Fig. 4. Maximum (positive) and minimum (negative) principal strain values at the medial, lateral, anterior and posterior surfaces of the bone-implant interface during (a) slow walking, (b) normal walking, (c) fast walking, (d) up stairs walking. The points in the curves correspond to the node positions along a line in the superior-inferior direction of the femur.

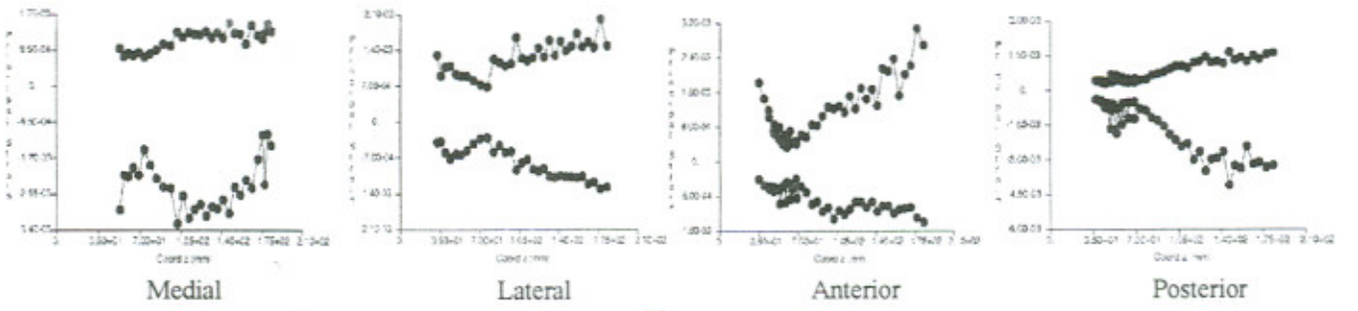

(e)

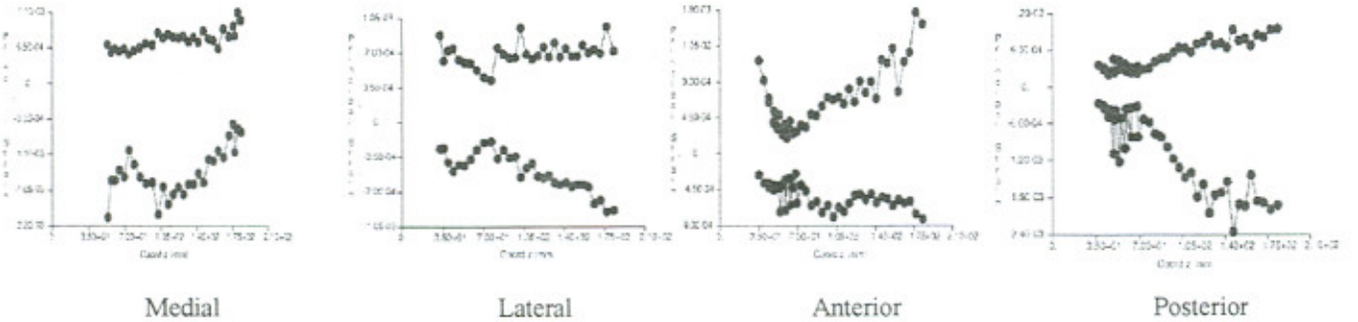

(f)

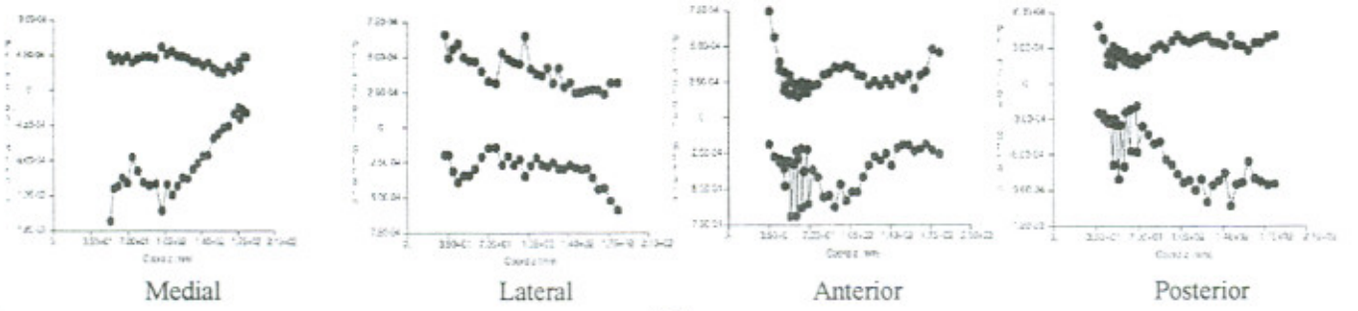

(g)

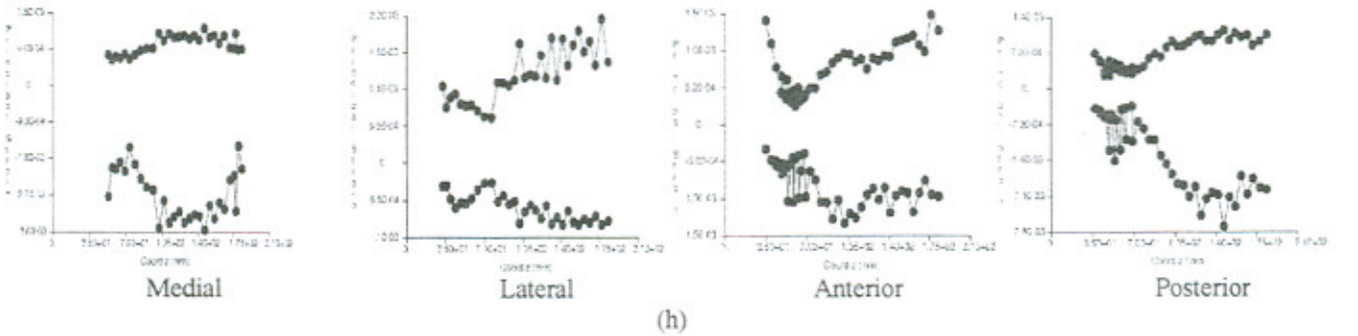

(h)

Fig. 4. (continued) Maximum and minimum principal strain values at the medial, lateral, anterior and posterior surfaces of the bone-implant interface during (e) down stairs walking, (f) standing up, (g) sitting down, (h) standing on 2-1-2 legs. The points in the curves correspond to the node positions along a line in the superior-inferior direction of the femur.

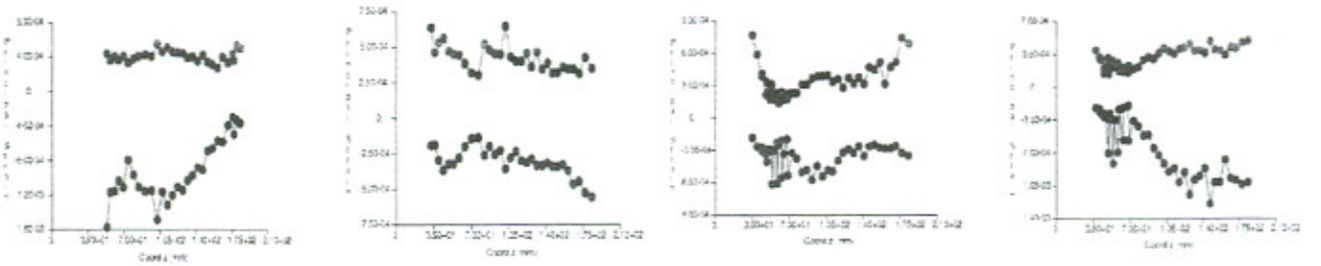

(i)

Fig. 4. (continued) Maximum and minimum principal strain values at the medial, lateral, anterior and posterior surfaces of the bone-implant interface during (i) knee bend. The points in the curves correspond to the node positions along a line in the superior-inferior direction of the femur.

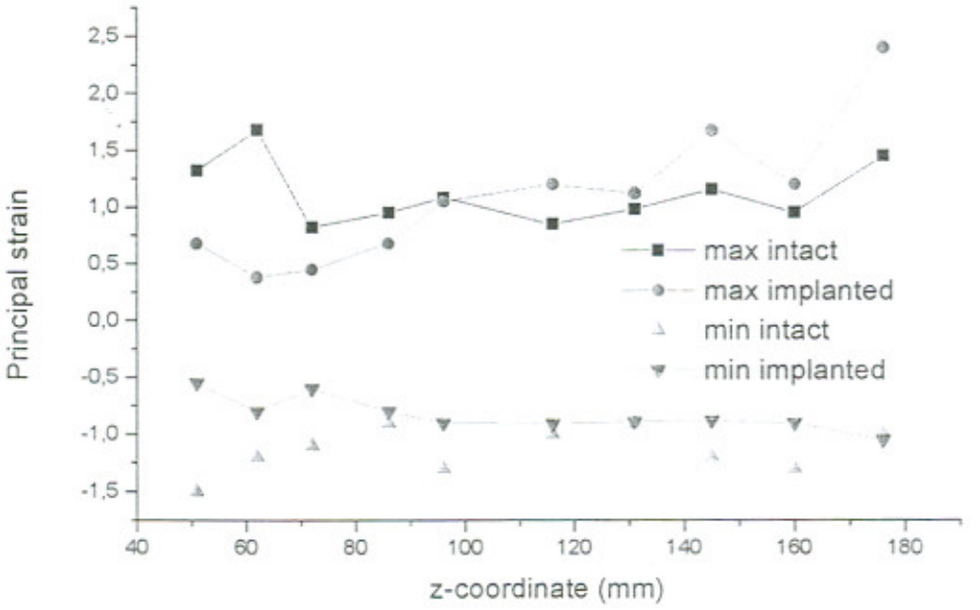

Fig. 5. Maximum and minimum principal strain values at nodal positions of the anterior surface of the bone-implant interface and at corresponding points of the intact femur model at the moment of peak hip contact force in walking. The points in the curves correspond to the node positions along a line in the superior-inferior direction of the femur.